Journal of Alloys and Compounds 732 (2018) 363–371

Contents lists available at ScienceDirect

Journal of Alloys and Compounds

journal homepage: http://www.elsevier.com/locate/jalcom

Complete dehydrogenation of hydrazine borane and hydrazine catalyzed by MIL-101 supported NiFePd nanoparticles

Kun Yang [a], Kangkang Yang [a], Shiliang Zhang [a], Yan Luo [b], Qilu Yao [a], Zhang-Hui Lu [a, *]

[a] Institute of Advanced Materials, College of Chemistry and Chemical Engineering, Jiangxi Normal University, Nanchang, 330022, China
[b] Department of Chemical Engineering, West Virginia University, WV, 26506, United States

ARTICLE INFO

Article history:
Received 13 June 2017
Received in revised form
25 October 2017
Accepted 26 October 2017
Available online 27 October 2017

Keywords:
Energy storage materials
Catalysis
Hydrogen production
Hydrazine borane
Nanoparticles

ABSTRACT

Trimetallic NiFePd nanoparticles (NPs) anchored on metal-organic framework (MOF) MIL-101 have been facilely prepared via a simple impregnation method. The as-prepared NiFePd/MIL-101 catalysts have been characterized by powder X-ray diffraction (XRD), scanning electron microscope (SEM), transmission electron microscope (TEM) equipped with energy dispersed X-ray detector (EDX) and selected area electron diffraction (SAED), inductively coupled plasma-atomic emission spectroscopy (ICP-AES), N_2 adsorption/desorption isotherms and X-ray photoelectron spectroscopy (XPS) techniques. And the as-synthesized catalysts have been applied for hydrogen generation from aqueous alkaline solution of hydrazine borane (HB, $N_2H_4BH_3$). Compared to the pure $Ni_{0.36}Fe_{0.24}Pd_{0.4}$ NPs, MIL-101 supported mono- and bi-metallic counterparts, the $Ni_{0.36}Fe_{0.24}Pd_{0.4}$/MIL-101 catalyst exhibits much higher catalytic performance for complete conversion of $N_2H_4BH_3$ to H_2 with 100% selectivity at 323 K. The turnover frequency (*TOF*) value for the dehydrogenation of $N_2H_4BH_3$ in the presence of $Ni_{0.36}Fe_{0.24}Pd_{0.4}$/MIL-101 catalyst reaches 60 h^{-1}. Remarkably, the $Ni_{0.36}Fe_{0.24}Pd_{0.4}$/MIL-101 catalyst also shows high catalytic activity and 100% selectivity towards hydrogen generation from hydrous hydrazine ($N_2H_4 \cdot H_2O$) at 323 K with a *TOF* value of 40.8 h^{-1}. In addition, the durability tests exhibit that the $Ni_{0.36}Fe_{0.24}Pd_{0.4}$/MIL-101 catalyst is still highly active in the complete dehydrogenation of $N_2H_4BH_3$ and decomposition of $N_2H_4 \cdot H_2O$ with 100% hydrogen selectivity even after five recycles.

1. Introduction

Hydrogen is generally regarded as one of the crucial alternative energy carriers to satisfy the increasing demand for a clean and a sustainable energy supply [1–3]. However, even after several decades of exploration, the development of safe and efficient methods for hydrogen storage materials still remains one of the most challenging barriers for hydrogen economy in the future [4–7]. Hydrazine borane (HB, $N_2H_4BH_3$) has been reported as a promising hydrogen storage medium due to its high hydrogen content (15.4 wt%), easy preparing and good stability in water [8–13]. The complete dehydrogenation of $N_2H_4BH_3$ can release 5 equivalents of H_2 via both hydrolysis of the BH_3 group (Eq. (1)) and complete decomposition of the N_2H_4 group of $N_2H_4BH_3$ to N_2 and H_2 (Eq. (2)) in the presence of a suitable catalyst [14,15], which corresponds to a theoretical gravimetric hydrogen storage capacity (GHSC) of 10.0 wt% for the system $N_2H_4BH_3$-$3H_2O$. However, in order to maximize the potency of $N_2H_4BH_3$ as a hydrogen storage material, the incomplete and undesired decomposition of hydrazine to ammonia (NH_3) via Eq. (3) should be avoided. Therefore, the development of efficient, highly selective and low cost catalysts is urgently important for promoting the practical application of $N_2H_4BH_3$ as a hydrogen storage material.

$$N_2H_4BH_3(s) + 3H_2O(l) \rightarrow N_2H_4(l) + B(OH)_3(l) + 3H_2(g) \quad (1)$$

$$N_2H_4(l) \rightarrow N_2(g) + 2H_2(g) \quad (2)$$

$$3N_2H_4(l) \rightarrow 4NH_3(g) + N_2(g) \quad (3)$$

So far, a number of catalyst systems have been tested for hydrogen generation from $N_2H_4BH_3$ [14–33]. Özkar and coworkers only focused on the hydrolysis of the BH_3 group of $N_2H_4BH_3$. However, only 3 equivalents of H_2 were released by hydrolysis of the BH_3 group of $N_2H_4BH_3$, which limited their further application. Several PtNi and RhNi catalysts can release 5

* Corresponding author.
E-mail address: luzh@jxnu.edu.cn (Z.-H. Lu).

https://doi.org/10.1016/j.jallcom.2017.10.241
0925-8388/

equivalents of H_2 per $N_2H_4BH_3$ by both hydrolysis of the BH_3 group and decomposition of the N_2H_4 group of $N_2H_4BH_3$ [25–27,30,33]. Recently, Demirci and co-workers reported that 4.3 equiv. ($H_2 + N_2$) per $N_2H_4BH_3$ was released in more than 180 min using the $Ni_{0.7}Pd_{0.3}$ catalyst, while $Ni_{0.7}Fe_{0.3}$ catalyst generated only 3.9 equiv. ($H_2 + N_2$) per $N_2H_4BH_3$ at 323 K [28].

Metal-organic frameworks (MOFs) are composed of metal ions as connecting center and organic molecular as linker, which can be regarded as a new class of promising porous materials [34]. Currently, MOFs have been employed for dispersion and stabilization of active metal NPs due to their high special surface area, uniform pores and chemical diversity [35–40]. In addition, MOFs can also afford the interactions between active metal NPs and organic ligands, which may further increase the catalytic activity [41,42].

Herein, we report a general and facile method for preparing trimetallic NiFePd NPs anchored on MIL-101 and further used as catalysts for hydrogen generation from aqueous alkaline solution of $N_2H_4BH_3$. Among all the catalysts, the $Ni_{0.36}Fe_{0.24}Pd_{0.4}$/MIL-101 catalyst exhibits the highest activity with 100% hydrogen selectivity toward the dehydrogenation of $N_2H_4BH_3$ at 323 K. Moreover, the $Ni_{0.36}Fe_{0.24}Pd_{0.4}$/MIL-101 catalyst also exhibits superior catalytic activity for the decomposition of N_2H_4.

2. Experimental

2.1. Materials

Hydrazine monohydrate ($N_2H_4 \cdot H_2O$, Aladdin, 98.0%), nickel (II) chloride hexahydrate ($NiCl_2 \cdot 6H_2O$, Sinopharm Chemical Reagent, ≥98.0%), ferric chloride hexahydrate ($FeCl_3 \cdot 6H_2O$, Sinopharm Chemical Reagent, ≥99.0%), palladium chloride ($PdCl_2$, Sinopharm Chemical Reagent, 99.99%), sodium borohydride ($NaBH_4$, J&K Scientific Ltd., 98%), aqueous hydrofluoric acid (HF, J&K Scientific Ltd., 40 wt.%), hydrazine hemisulfate salt ($N_2H_4 \cdot 1/2H_2SO_4$, Sigma-Aldrich, >99.5%), n-pentane (C_5H_{12}, Sigma-Aldrich, 99.5%), 1,4-dioxane ($C_4H_8O_2$, J&K Scientific Ltd., 99.8%), chromic nitrate nonahydrate ($Cr(NO_3)_3 \cdot 9H_2O$, Aladdin, 99.9%), *p*-phthalic acid ($HO_2CC_6H_4CO_2H$, Aladdin, 99%), sodium hydroxide (NaOH, Tianjin Fuchen Chemical Reagent, ≥96.0%), and hydrochloric acid (HCl, Tianjin Fuchen Chemical Reagent, 36–37%) were employed without further purification. Ultrapure water (R = 18 MΩ cm) was obtained by reversed osmosis followed by ion exchanged and filtration.

2.2. Synthesis of $N_2H_4BH_3$

Hydrazine borane ($N_2H_4BH_3$) was synthesized according to the previous reports [8,26]. Briefly, hydrazine hemisulfate salt (21.42 g) and sodium borohydride (10 g) were suspended in anhydrous dioxane (80 mL), and kept stirring for 48 h under Ar atmosphere. Afterwards, the mixture was separated by centrifugation at 12000 rpm for 12 min. Then, the solvent was removed under vacuum at 313 K overnight and *n*-pentene was added to precipitate $N_2H_4BH_3$. Finally, the precipitate was separated by centrifugation, washed with *n*-pentene for several times, and dried under vacuum at 313 K.

2.3. Synthesis of MIL-101

MIL-101 was synthesized according to the reported procedure [39]. Typically, 1.661 g of *p*-phthalic acid, 4.002 g of $Cr(NO_3)_3 \cdot 9H_2O$, 0.6 mL of aqueous HF and 70 mL of water were transferred to a 100 mL Teflon-liner autoclave, which was then heated at 473 K for 8 h. After natural cooling, the resulting green powder with formula $Cr_3F(H_2O)_2[(O_2C)C_6H_4(CO_2)]_3 \cdot nH_2O$ was filtered off using a large pore fritted glass filter. The resulting green powder was washed thoroughly with hot water and ethanol, and then soaked in ethanol at 373 K for 24 h for twice and washed by hot ethanol. The resulting green powder was finally dried at 423 K overnight under vacuum for further use.

2.4. Synthesis of NiFePd/MIL-101

NiFePd/MIL-101 was synthesized by the simple liquid impregnation method. Typically, MIL-101 (100 mg) was mixed with 5 mL ultrapure water and sonicated for 30 min to obtain a fully dispersed suspension. $NiCl_2 \cdot 6H_2O$ (17.46 mg), $FeCl_3 \cdot 6H_2O$ (13.10 mg), and $PdCl_2$ (14.2 mg) were dissolved in 5 mL aqueous solution by vigorous stirring, and then the aqueous solution of metal slats was added to the above solution. The mixed solution was stirred vigorously at room temperature for 8 h. Subsequently, 50 mg of $NaBH_4$ was quickly added as reducing agent into the above solution with vigorous stirring until no more gas generation. Finally, the resulting black products of $Ni_{0.36}Fe_{0.24}Pd_{0.4}$/MIL-101 could be obtained and then directly used for catalytic reaction. The mono-/bimetallic counterparts and NiFePd/MIL-101 with different compositions (n_{metal} = 0.2 mmol) were synthesized by the same method as described above.

2.5. Catalysts characterization

The powder X-ray diffraction (XRD) was recorded on a Rigaku RINT-2200 X-ray diffractometer with a Cu Kα source (40 kV, 20 mA). The surface topography of the samples was investigated by scanning electron microscope (SEM, SU-8020) and transmission electron microscope (TEM, JEM-2100) equipped with energy dispersed X-ray detector (EDX) and selected area electron diffraction (SAED) analysis. The TEM samples were prepared by depositing one or two droplets of the catalysts suspensions on the carbon coated copper grids. The metal content in catalysts was determined by inductively coupled plasma-atomic emission spectroscopy (ICP-AES). The specific surface area measurements were obtained from N_2 adsorption/desorption isotherms at 77 K after dehydration under vacuum at 423 K for 10 h using BELSORP-mini II. X-ray photoelectron spectroscopy (XPS) measurement was carried out on a VG Escalabmkll spectrometer with a Al K_α source.

2.6. Catalytic reactions

The catalytic performance of the as-prepared catalysts for hydrogen generation from $N_2H_4BH_3$ or $N_2H_4 \cdot H_2O$ was tested in a typical water-filled graduated buret system. Typically, the as-prepared catalysts suspension (5 mL, n_{metal} = 0.2 mmol) and NaOH (2.0 M) were dissolved in a two-necked round-bottomed flask, which was placed in a water bath at 323 K under ambient atmosphere. A trap filled with HCl (0.1 M) solution was placed between the reactor and the inverted gas buret filled with water (to ensure absorption of any evolving ammonia (NH_3)). To start the catalytic reaction, $N_2H_4BH_3$ or $N_2H_4 \cdot H_2O$ (1 mmol) was added to the catalyst suspension and the volume of H_2 along N_2 was measured by the gas buret, from which the molar ratio $\lambda = n_{(H2+N2)}/n_{(N2H4BH3)}$ or $\gamma = n_{(H2+N2)}/n_{(N2H4 \cdot H2O)}$ was obtained. The selectivity (α) towards hydrogen generation from $N_2H_4BH_3$ can be evaluated using Eq. (4), which can be derived from equations (1)–(3). Therefore, the selectivity α was defined as Eq. (5). The selectivity for hydrogen generation (β) from decomposition of $N_2H_4 \cdot H_2O$ can be calculated by using Eq. (6).

$$N_2H_4BH_3 + 3H_2O \rightarrow B(OH)_3 + (3+2\alpha)H_2 + (2\alpha+1)/3N_2 + 4(1-\alpha)/3NH_3 \quad (4)$$

$$\alpha = \frac{3\lambda - 10}{8} \quad \left[\lambda = \frac{n(H_2 + N_2)}{n(HB)}\left(\frac{10}{3} \le \lambda \le 6\right)\right] \tag{5}$$

$$\beta = \frac{3\gamma - 1}{8} \quad \left[\gamma = \frac{n(H_2 + N_2)}{n(N_2H_4)}\left(\frac{1}{3} \le \gamma \le 3\right)\right] \tag{6}$$

2.7. Durability test

For durability tests, after the completion of the first run of hydrogen generation, another equivalent of $N_2H_4BH_3$ (or $N_2H_4 \cdot H_2O$) and NaOH was subsequently added to the reaction system and the released gas was monitored by the gas buret. The durability test for the catalytic dehydrogenation of $N_2H_4BH_3$ (or $N_2H_4 \cdot H_2O$) was carried out for five runs at 323 K.

3. Results and discussion

3.1. Preparation and characterization

A simple impregnation method, followed by co-reduction of the metal salts, was applied to synthesize trimetallic NiFePd/MIL-101 catalyst. The as-prepared samples were characterized by XRD, SEM, TEM, SAED, EDX, ICP-AES, N_2 adsorption-desorption, and XPS techniques. Fig. 1 shows the small-angle and wide-angle power XRD patterns of MIL-101, Ni/MIL-101, Fe/MIL-101, Pd/MIL-101, and NiFePd/MIL-101, respectively. The small-angle PXRD patterns (Fig. 1a) show that the intrinsic structure of MIL-101 is maintained well during the synthesis of MIL101 supported metal NPs. From the wide-angle pattern of the PXRD of the as-synthesized samples (Fig. 1b), the characteristic diffraction peak of Fe/MIL-101 at 44.7° can be attributed to (111) plane of Fe (JPCDS No.06-0696). The diffraction peaks of Pd/MIL-101 appearing at 39.5° and 45.9° can be ascribed to (111) and (200) planes of Pd (JPCDS No.05-0681), respectively. The PXRD pattern of Ni/MIL-101 shows no diffraction peak, probably due to the amorphous structure of Ni NPs. As for NiFePd/MIL-101 sample, no obvious characteristic diffraction peak of metal NPs is observed, indicating the formation of the amorphous structure (which can be evidenced later by the SAED result). As shown in Fig. S1, after heat treatment at 823 K for 3 h in Ar atmosphere, NiFePd/MIL-101 sample is well crystallized and the unit cell parameter (a) is between the values for Ni (JPCDS No.04-0850), Fe (JPCDS No.06-0696) and Pd (JPCDS No.05-0681). In addition, the crystalline Ni is also formed in Ni/MIL-101 sample after heat treatment at 823 K for 3 h under Ar atmosphere (Fig. S2).

The morphologies of original MIL-101 and NiFePd/MIL-101 were characterized by scanning electron microscope (SEM) and transmission electron microscope (TEM). SEM images of MIL-101 (Fig. S3) and NiFePd/MIL-101 (Fig. 2a) indicate that the octahedral structure of the MIL-101 framework is maintained well after loading the NiFePd NPs, in line with the corresponding PXRD results (Fig. 1). As shown in Fig. 2b, the octahedral structure of the MIL-101 framework can be also observed in the TEM image of NiFePd/MIL-101. The size and distribution of NiFePd NPs were characterized by TEM. TEM images presented in Fig. 2c show that the NiFePd NPs are highly dispersed with a small size of about 2–3 nm. The corresponding selected area electron diffraction (SAED) pattern (inset Fig. 2c) confirms an amorphous structure. Moreover, the corresponding energy dispersive X-ray (EDX) spectrum (Fig. 2d) confirms the existence of Ni, Fe, Pd, and Cu elements in the as-prepared catalysts, where the Cu element is ascribed to the carbon coated Cu grids. The accurate molar ratio of Ni: Fe: Pd is determined to be 36: 24: 40 by the inductively coupled plasma atomic emission spectroscopic (ICP-AES), which is quite close to their initial atomic ratio (Table S1). The N_2 absorption/desorption isotherms of MIL-101 and NiFePd/MIL-101 catalysts have been carried out at 77 K (Fig. S4). The Brunauer-Emmett-Teller (BET) surface areas of the MIL-101 and NiFePd/MIL-101 catalysts are estimated to be 3186 and 2422 m_2/g, respectively. Compared with the MIL-101, the drastic decrease in the surface area of NiFePd/MIL-101 indicates that the cavities and/or surface of MIL-101 are occupied and blocked by the highly dispersed metal NPs.

In order to understand the valence state and surface composition of $Ni_{0.36}Fe_{0.24}Pd_{0.4}$/MIL-101 catalysts, X-ray photoelectron spectroscopy (XPS) analyses after Ar sputtering were carried out. Fig. 3a shows the full scanning survey spectrum ranging from 0 to 1200 eV. The peaks of Ni, Fe, Pd, Cr, F, C, and O elements are clearly observed in this XPS spectrum. Ni 2p spectra shown in Fig. 3b have two peaks with binding energies of 852.9 and 872.3 eV, which are assigned to $2p_{3/2}$ and $2p_{1/2}$ of metallic Ni, respectively. Fig. 3c shows the Fe 2p spectrum and the peaks at binding energies of 707.4 and 720.6 eV can be assigned to metallic Fe, while the peaks at binding energies of 710 and 723.7 eV are attributed to oxidized Fe. The formation of the oxidized Fe was probably due to the exposure of the surface Fe to atmospheric oxygen during the catalyst preparation process. For the Pd 3d spectrum, it can be seen that the peaks at

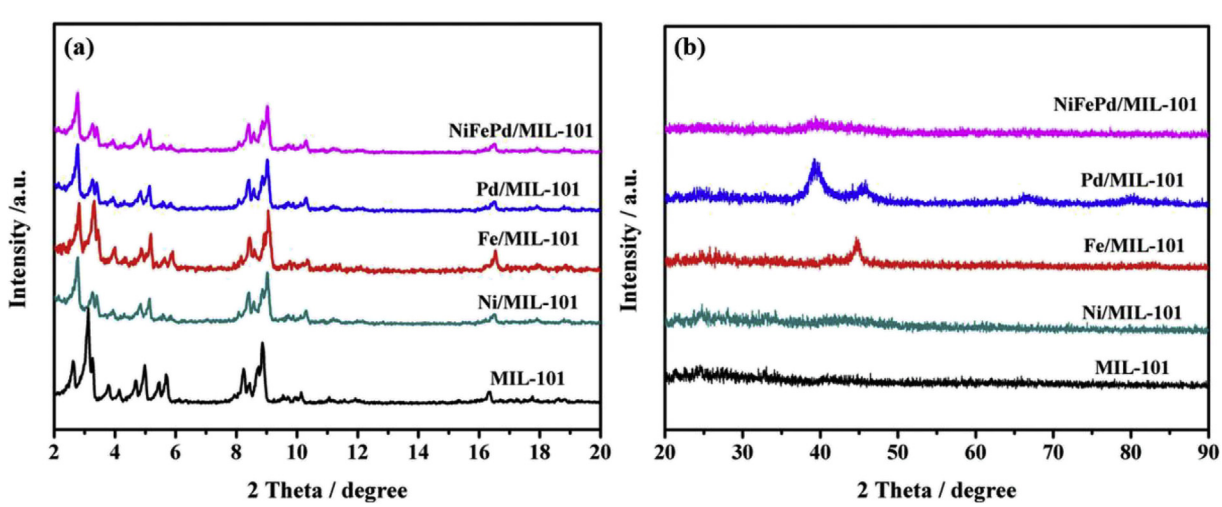

Fig. 1. (a) Small-angle and (b) wide-angle PXRD patterns of the as-prepared MIL-101, Ni/MIL-101, Fe/MIL-101, Pd/MIL-101, and $Ni_{0.36}Fe_{0.24}Pd_{0.4}$/MIL-101.

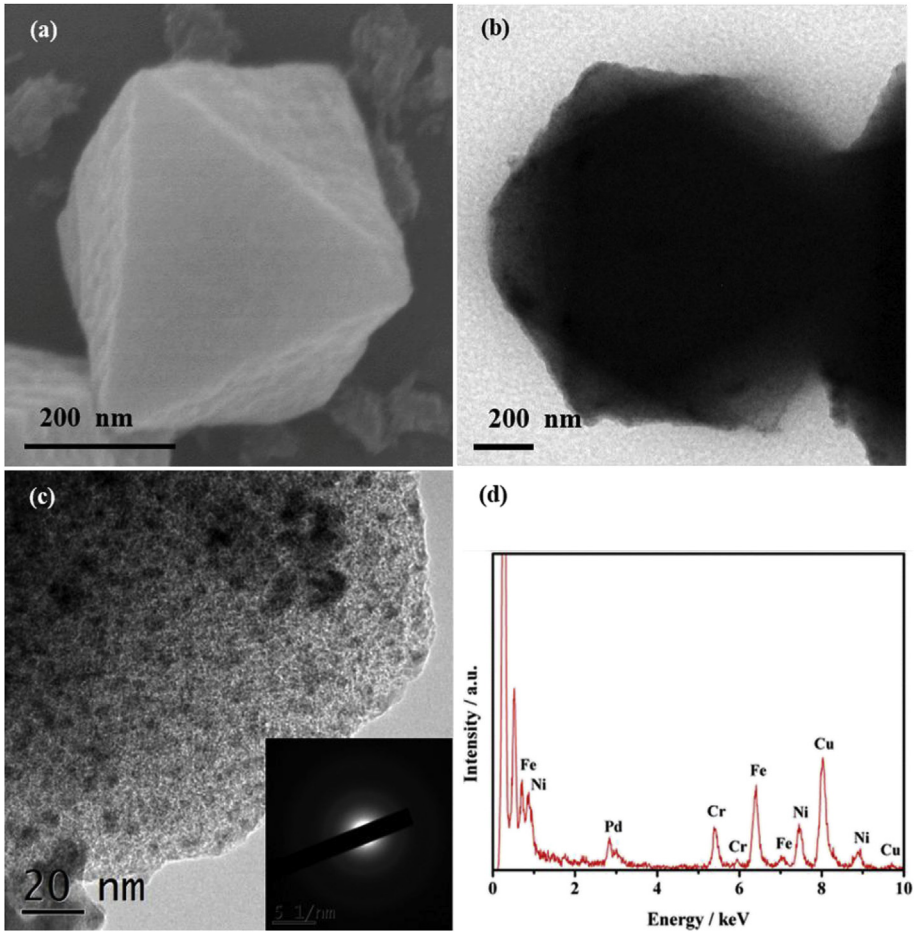

Fig. 2. (a) Typical SEM image, (b, c) TEM images and (inset) the corresponding SAED pattern, and (d) EDX spectrum of $Ni_{0.36}Fe_{0.24}Pd_{0.4}$/MIL-101 catalyst.

335.8 and 341.1 eV are assigned to the $3d_{5/2}$ and $3d_{3/2}$ of the metallic Pd (Fig. 3d). In addition, the binding energy of metallic Ni $2p_{3/2}$ (852.9 eV) in $Ni_{0.36}Fe_{0.24}Pd_{0.4}$/MIL-101 catalyst is shifted to a lower value as compared to that of Ni/MIL-101 catalyst (853.3 eV). At the same time, the binding energies of Fe $2p_{3/2}$ (707.5 eV) and Pd $3d_{5/2}$ (336.3 eV) in $Ni_{0.36}Fe_{0.24}Pd_{0.4}$/MIL-101 catalyst are shifted to a higher value as compared to that of Fe/MIL-101 (707.3 eV) and Pd/MIL-101 catalyst (336 eV), respectively. These shifts of the binding energies are due to the slight electron transfer from Fe and Pd to Ni. Such electronic interaction between Ni, Fe and Pd in the $Ni_{0.36}Fe_{0.24}Pd_{0.4}$/MIL-101 catalyst may lead to an improved catalytic performance for hydrogen generation from $N_2H_4BH_3$. Thus, the above XPS results provide a certain evidence for the formation of the alloy NiFePd in $Ni_{0.36}Fe_{0.24}Pd_{0.4}$/MIL-101 catalyst. Moreover, the peaks with binding energies of 587.2 and 577.4 eV in pure MIL-101 and metal NPs/MIL-101 composites can be assigned to the Oxidized Cr of MIL-101 (Fig. S5a). Fig. S5b shows XPS spectra for O 1s in as-prepared catalysts, with a peak centred at 532.4 eV. The O1s spectra in Fig. S5b showed a peak centred at 532.4 eV, which can be attributed to adsorbed water and/or an oxygen-containing carbon compound in MIL-101.

3.2. Catalytic performance

The catalytic activities of the as-synthesized catalysts have been evaluated for the hydrogen evolution from $N_2H_4BH_3$ at 323 K in alkaline solution (2.0 M). Clearly, the hydrogen selectivity and catalytic activity are significantly dependent on the metallic compositions of the catalysts. As shown in Fig. 4a, the catalytic performances of the $(Ni_{0.5}Fe_{0.5})_{1-x}Pd_x$/MIL-101 catalysts increase when the Pd molar ratio (x value) increases from 0.1 to 0.4. Subsequently, further increase of the Pd content decreases the catalytic activity. As a result, the best Pd molar ratio ($x = 0.4$) in the $(Ni_{0.5}Fe_{0.5})_{1-x}Pd_x$/MIL-101 catalysts is 0.4. On the other hand, the effect of the amount of Ni and Fe has also been studied by changing the molar ratio Ni/Fe in $(Ni_{1-y}Fe_y)_{0.6}Pd_{0.4}$/MIL-101 catalysts. As shown in Fig. 4b, the best molar ratio of Ni/Fe is 3/2 (i.e., $y = 0.4$). The $Ni_{0.36}Fe_{0.24}Pd_{0.4}$/MIL-101 catalyst exhibits the highest catalytic performance among all the as-synthesized catalysts with different metallic compositions. A high turnover frequency (*TOF*) value of 60 h^{-1} at 323 K is obtained for dehydrogenation of $N_2H_4BH_3$, which is higher than those of Ni_5@Pt [23], $Ni_{0.7}Pd_{0.3}$ [28], $Ni_{0.89}Ir_{0.11}$ [17], $Ni_{0.89}Rh_{0.11}$ [17], and $Ni_{0.77}Ru_{0.23}$ [17] catalysts and lower than the values for Ni@(Rh_4Ni-alloy)/Al_2O_3 [20], Rh_4Ni [18], $Ni_{0.6}Pt_{0.4}$/MSC-30 [25], and $Rh_{0.8}Ni_{0.2}$@CeO_x/rGO [30] catalysts (Table S2). Pd NPs stabilized by PVP produced only 3 equivalents of hydrogen [24], indicating that it is only active in hydrolysis of BH_3 group of $N_2H_4BH_3$.

For comparison, the catalytic performances of the same amounts of as-prepared mono-/bi-metallic counterparts for the hydrogen generation from $N_2H_4BH_3$ were evaluated. As shown in Fig. 5a, it can be seen that the monometallic Ni/MIL-101, Fe/MIL-101, and Pd/MIL-101 show a low activity for the hydrogen generation from $N_2H_4BH_3$ at 323 K, generating 4.29, 2.7 and 3.0 equiv. ($H_2 + N_2$) per $N_2H_4BH_3$ within 170, 98.17 and 0.33 min, respectively. Among all the monometallic catalysts, only Ni/MIL-101 catalysts

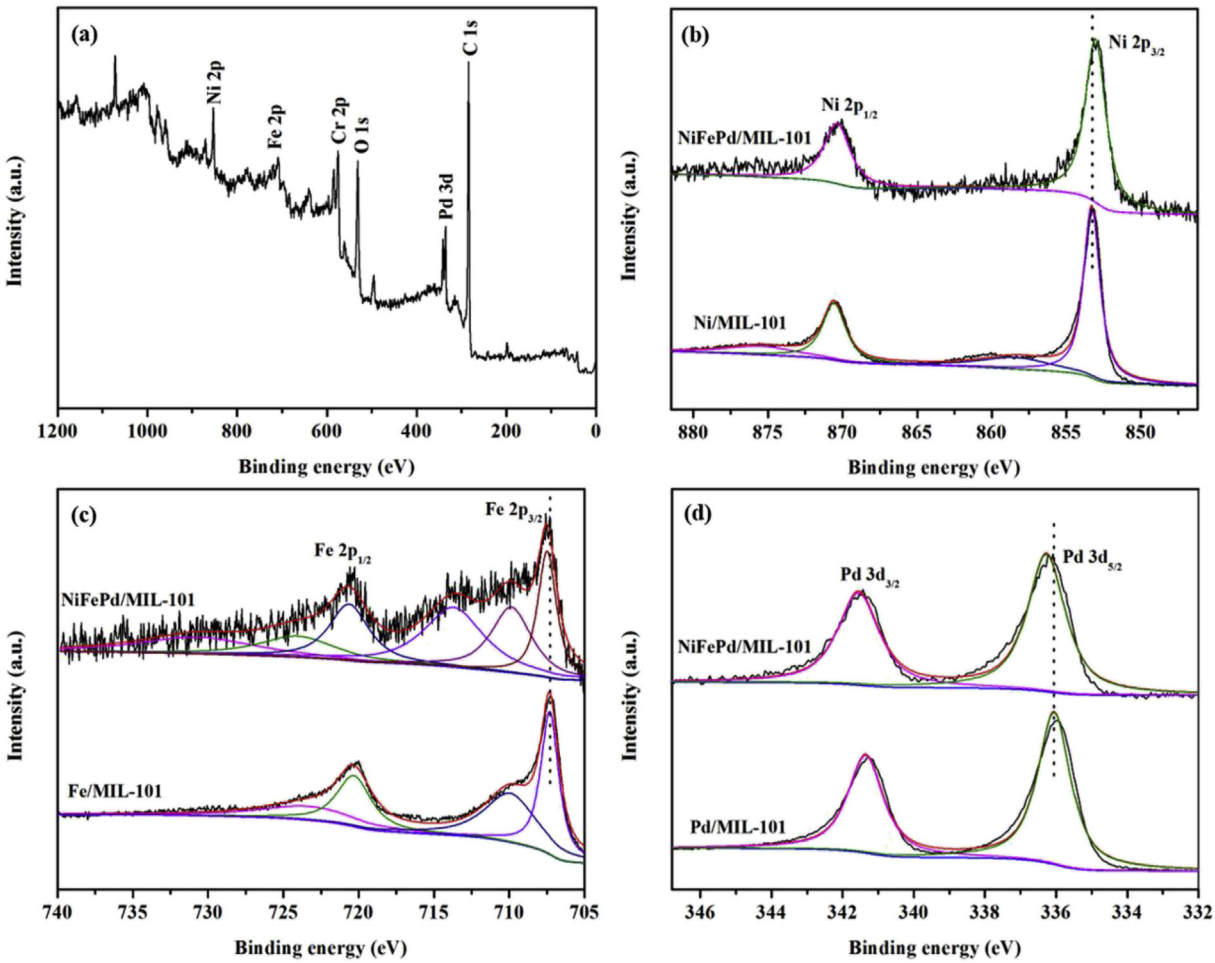

Fig. 3. (a) The survey XPS spectrum of $Ni_{0.36}Fe_{0.24}Pd_{0.4}$/MIL-101; XPS spectra of (b) Ni 2p, (c) Fe 2p, and (d) Pd 3d for the synthesized catalysts.

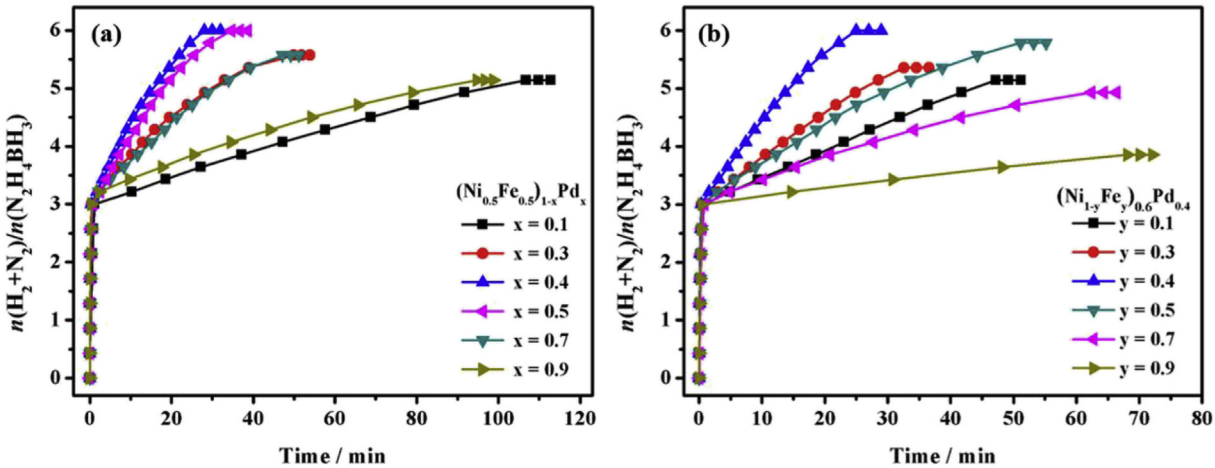

Fig. 4. Time plots for H_2 generation from $N_2H_4BH_3$ (0.2 M, 5 mL) catalyzed by (a) $(Ni_{0.5}Fe_{0.5})_{1-x}Pd_x$/MIL-101 and (b) $(Ni_{1-y}Fe_y)_{0.6}Pd_{0.4}$/MIL-101 catalysts in the presence of NaOH (2.0 M) at 323 K ($n_{metal}/nN_2H_4BH_3 = 0.2$ mmol).

can cause the N_2H_4 moiety of $N_2H_4BH_3$ to release H_2. In addition, the as-synthesized bimetallic NiFe/MIL-101, NiPd/MIL-101, and FePd/MIL-101 show higher catalytic activity and selectivity for hydrogen generation from $N_2H_4BH_3$ than that of monometallic counterparts, releasing 4.89, 5.14 and 3.0 equiv. (H_2 + N_2) per $N_2H_4BH_3$ in 124, 30.07 and 0.27 min, respectively. These mono-/bi-metallic counterparts can not force $N_2H_4BH_3$ to completely release H_2. However, 6.0 equiv. of (H_2 + N_2) per $N_2H_4BH_3$ is generated within only 25 min in the presence of $Ni_{0.36}Fe_{0.24}Pd_{0.4}$/MIL-101 catalyst. The significantly enhanced catalytic performance of

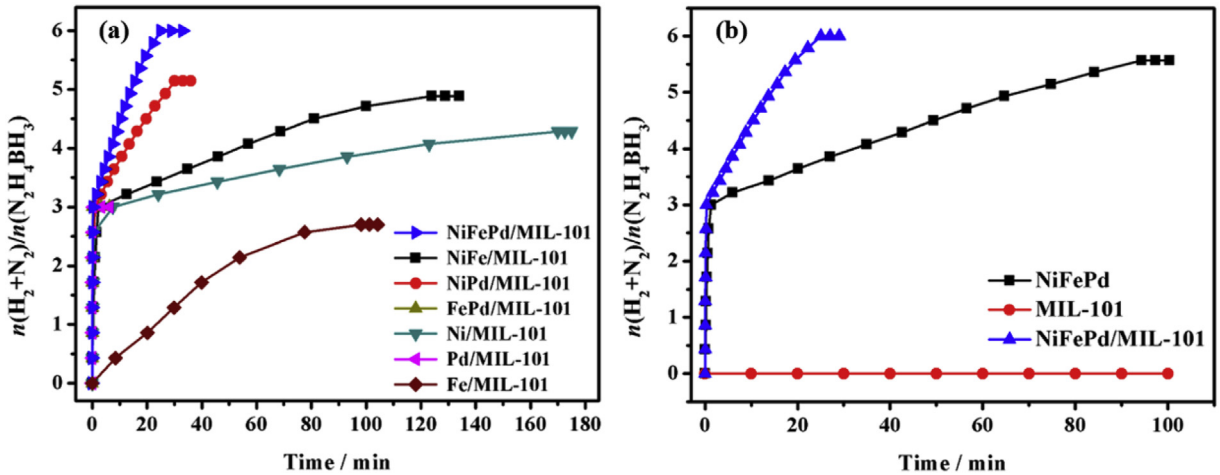

Fig. 5. Time plots for H_2 generation from $N_2H_4BH_3$ catalyzed by different catalysts ($n_{metal}/nN_2H_4BH_3$ = 0.2 mmol) in the presence of NaOH (2.0 M) at 323 K.

$Ni_{0.36}Fe_{0.24}Pd_{0.4}$/MIL-101 catalyst is probably due to the synergistic effects between Ni, Fe and Pd. Furthermore, in order to study the effect of porous MIL-101 on hydrogen generation, the catalytic performances of $Ni_{0.36}Fe_{0.24}Pd_{0.4}$ NPs, MIL-101, and $Ni_{0.36}Fe_{0.24}Pd_{0.4}$/MIL-101 catalysts were evaluated. As shown in Fig. 5b, 5.5 equiv. ($H_2 + N_2$) per $N_2H_4BH_3$ is generated in more than 94 min in the presence of the pure $Ni_{0.36}Fe_{0.24}Pd_{0.4}$ NPs, while no activity is observed for MIL-101. These results indicate that the strong interaction between trimetallic NPs and MIL-101 is required for hydrogen evolution from $N_2H_4BH_3$.

Previous researches have shown that the presence of NaOH had a promoting effect on the catalytic performance of $N_2H_4BH_3$ dehydrogenation [26]. To investigate the effect of NaOH, hydrogen generation from $N_2H_4BH_3$ with the addition of different amounts of NaOH has been comparatively studied. As shown in Fig. S6, $Ni_{0.36}Fe_{0.24}Pd_{0.4}$/MIL-101 catalyst without NaOH additive releases 3.0 equiv. of gases per $N_2H_4BH_3$. However, the selectivity and catalytic activity of $Ni_{0.36}Fe_{0.24}Pd_{0.4}$/MIL-101 catalyst increase when increasing the NaOH concentration from 0 to 2.0 M, but further increases the NaOH concentration has no obvious effect on the catalytic performance. These results confirm that NaOH can serve as a catalyst promoter for hydrogen generation from $N_2H_4BH_3$. The possible reason for the promoting effect of NaOH might be understood as follows: the existence of NaOH can efficiently decrease the concentration of undesirable $N_2H_5^+$ ($N_2H_5^+ + OH^- \rightarrow N_2H_4 + H_2O$) and to accelerate the rate-determining deprotonation step ($N_2H_4 \rightarrow N_2H_3^* + H^*$) in the decomposition process of N_2H_4 [43,44]. In addition, the alkaline environment can also suppress the generation of basic product NH_3, which increases the hydrogen selectivity [45].

In order to obtain the activation energy (E_a) of $Ni_{0.36}Fe_{0.24}Pd_{0.4}$/MIL-101 catalyst for the two distinct steps of dehydrogenation of $N_2H_4BH_3$, the reactions were carried out at different temperatures ranging from 313 to 353 K. As shown in Fig. 6a, the hydrogen generation rate increases by increasing the reaction temperature, indicating that a high reaction temperature is beneficial for increasing the hydrogen generation rate. The values of rate constant k at different temperatures were calculated from the slope of the linear part in Fig. 6a. According to the Arrhenius plot (ln k vs 1/T), the E_{a1} value for the hydrolysis of the BH_3 group and E_{a2} value for the decomposition of the N_2H_4 moiety are estimated to be 30.3 and 58.1 kJ/mol, respectively (Fig. 6b).

As shown Figs. 4–6, the gas generation curve from $N_2H_4BH_3$ shows a distinct two-step process, with a fast gas generation due to the hydrolysis of BH_3 group followed by a reaction with slower kinetics due to the dehydrogenation of N_2H_4 moiety of $N_2H_4BH_3$, which is consistent with the previous reports [14]. The hydrolysis of BH_3 group in $N_2H_4BH_3$ was reported to be as a zero-order reaction with respect to $N_2H_4BH_3$ concentration in the previous work [31]. We deduced that the kinetics of the dehydrogenation of the N_2H_4 moiety in $N_2H_4BH_3$ is similar to that of the decomposition of N_2H_4, which proceeds as a near zero-order kinetics at a concentration of 0.2 M (*vide infra*).

Furthermore, as a closely related compound, hydrous hydrazine ($N_2H_4 \cdot H_2O$) has been reported as another potential hydrogen carrier due to its high hydrogen storage capacity (8.0 wt%), high stability, relatively low cost, and easy recharging ability [46–50]. The development of a suitable and efficient catalyst for hydrogen generation from the decomposition of $N_2H_4 \cdot H_2O$ is highly desired. In this work, the optimized $Ni_{0.36}Fe_{0.24}Pd_{0.4}$/MIL-101 catalyst was also employed as an efficient catalyst for the decomposition of $N_2H_4 \cdot H_2O$ under the same conditions. As shown in Fig. 6c, the catalytic reactions for the decomposition of $N_2H_4 \cdot H_2O$ catalyzed by $Ni_{0.36}Fe_{0.24}Pd_{0.4}$/MIL-101 catalyst are completed in 63.8, 29.4, 15.93, 11.9 and 6.65 min at 313, 323, 333, 343 and 353 K (Fig. 6c), respectively, corresponding to the *TOF* values of 18.8, 40.8, 75.3, 100.8 and 180.5 h^{-1}. These *TOF* values are higher than those reported for the Pd-based catalysts for the decomposition of $N_2H_4 \cdot H_2O$ at various temperatures (Table S3) [30,43–45,54–66]. The E_a value for the decomposition of the N_2H_4 is estimated to be 51.4 kJ/mol (Fig. 6d). It is noted that the gas generation curves in each plot first rise linearly and then show a short plateau at the end of the reaction over the $Ni_{0.36}Fe_{0.24}Pd_{0.4}$/MIL-101 catalyst. Similar features were also observed in the previous reports [43–53]. It was found that the catalytic decomposition of $N_2H_4 \cdot H_2O$ follows a near zero-order kinetics at the initial reaction stage with a high N_2H_4 concentration (0.08 M–5.0 M) and then a first-order kinetics at a small $N_2H_4 \cdot H_2O$ concentration (0.01–0.08 M) [48,51–53]. Thus, the short plateau at the end of the reaction in the gas generation curves is probably due to the very low hydrogen release rate resulting from the very small N_2H_4 concentration as the catalytic reaction proceeds.

The recycle stability of the catalyst is crucial in the practical applications, therefore, the durability tests of $Ni_{0.36}Fe_{0.24}Pd_{0.4}$/MIL-101 catalyst were carried out at 323 K by adding the same amount of $N_2H_4BH_3$ and $N_2H_4 \cdot H_2O$ (1 mmol) into the reaction flask after the completion of the previous run. Fig. 7 shows the volume of hydrogen evolution versus the reaction time during the durability

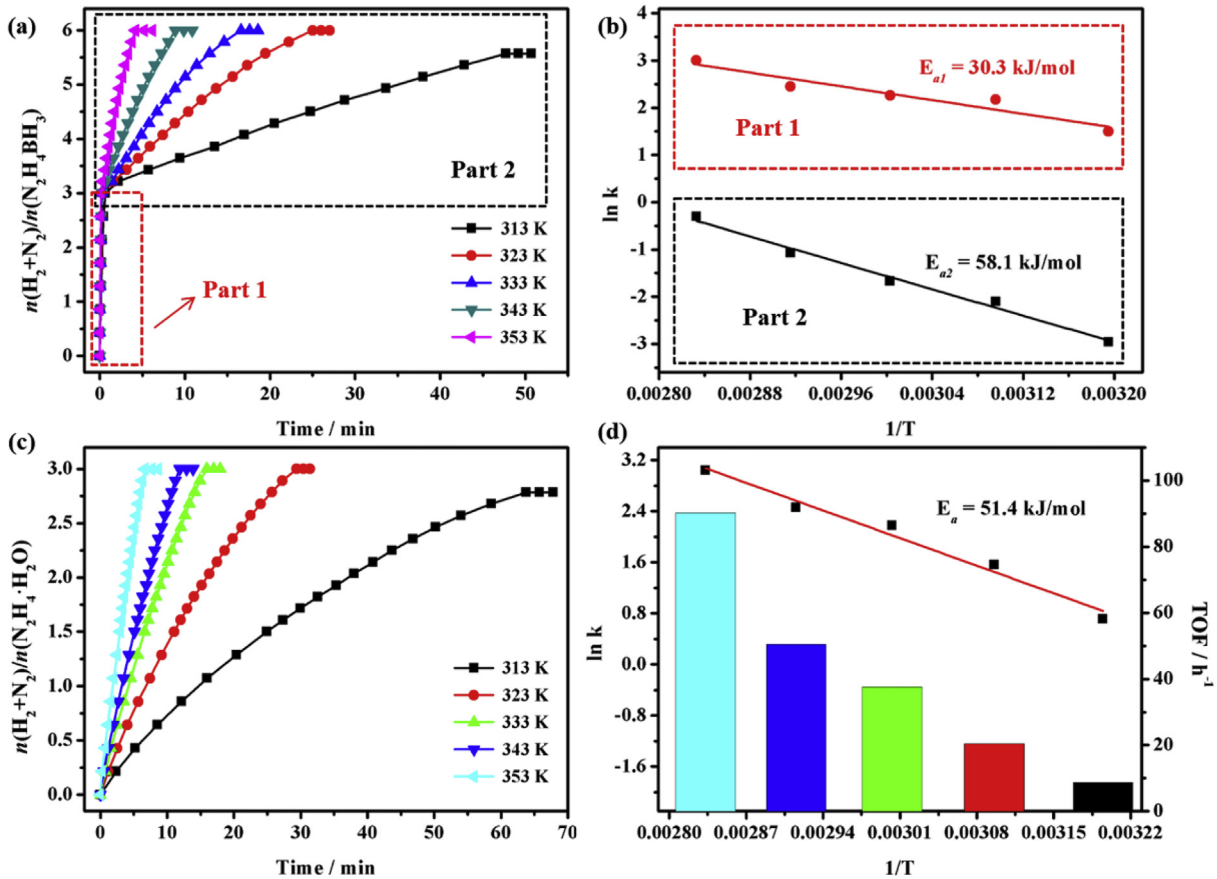

Fig. 6. Time plots for H_2 generation from aqueous solution of (a) $N_2H_4BH_3$ and (c) N_2H_4 catalyzed by $Ni_{0.36}Fe_{0.24}Pd_{0.4}$/MIL-101 in the presence of NaOH (2.0 M) at different temperatures ($n_{metal}/nN_2H_4BH_3$ = 0.2 mmol). Plot of ln k versus 1/T during the release of H_2 from (b) the dehydrogenation of the BH_3 (Part 1) and N_2H_4 moiety (Part 2) of $N_2H_4BH_3$ and (d) the decomposition of N_2H_4 aqueous solution catalyzed by $Ni_{0.36}Fe_{0.24}Pd_{0.4}$/MIL-101 at different temperatures.

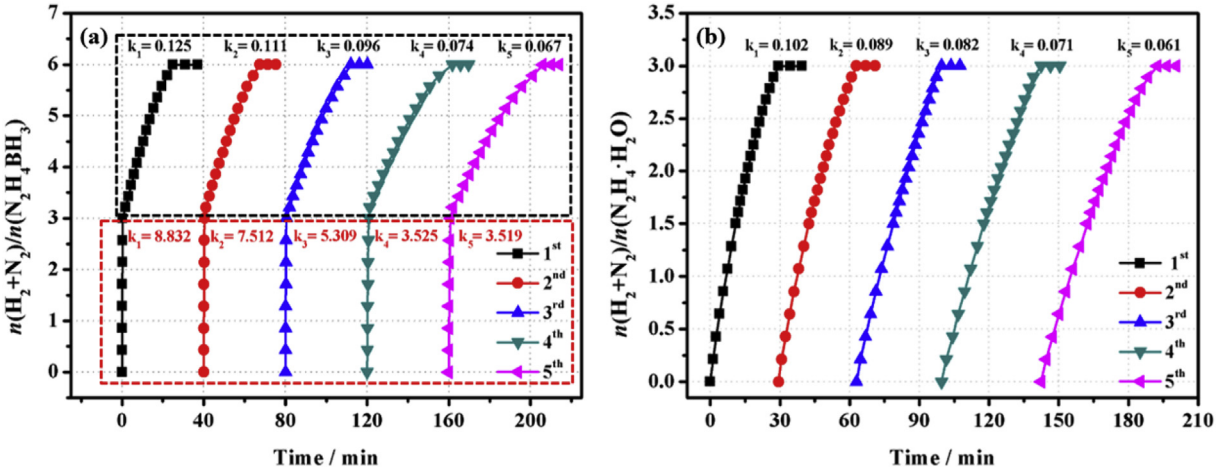

Fig. 7. Durability test for H_2 generation from aqueous solution of (a) $N_2H_4BH_3$ and (b) N_2H_4 (1.0 mmol) over $Ni_{0.36}Fe_{0.24}Pd_{0.4}$/MIL-101 ($n_{metal}/n(N_2H_4BH_3$ or $N_2H_4)$ = 0.2 mmol) in the presence of NaOH (2.0 M) at 323 K.

tests of $Ni_{0.36}Fe_{0.24}Pd_{0.4}$/MIL-101 catalyst for the dehydrogenation of $N_2H_4BH_3$ and $N_2H_4 \cdot H_2O$ at 323 K. After five cycles, hydrogen selectivity remains unchanged, and only a slight decrease of the activity for hydrogen generation from $N_2H_4BH_3$ and $N_2H_4 \cdot H_2O$ is observed, indicating a good durability of the $Ni_{0.36}Fe_{0.24}Pd_{0.4}$/MIL-101 catalyst.

4. Conclusions

MIL-101 supported Ni, Fe, Pd, NiFe, NiPd, FePd, NiFePd catalysts have been synthesized using a facile impregnation method. All the as-synthesized catalysts are active for the hydrolysis of the BH_3 group of $N_2H_4BH_3$. MIL-101 supported Ni, NiFe, and NiPd catalysts

show a limited reactivity towards the N_2H_4 moiety, while Fe, Pd, and FePd catalysts do not show any reactivity. Compared to the monometallic and bimetallic counterparts, the trimetallic $Ni_{0.36}Fe_{0.24}Pd_{0.4}$/MIL-101 catalyst exhibit the best catalytic performance with 100% hydrogen selectivity towards hydrogen generation from alkaline solution of $N_2H_4BH_3$ and N_2H_4 at 323 K. The *TOF* values for $Ni_{0.36}Fe_{0.24}Pd_{0.4}$/MIL-101 catalyst in the dehydrogenation of $N_2H_4BH_3$ and N_2H_4 reach 60 and 40.8 h^{-1}, respectively. Moreover, the $Ni_{0.36}Fe_{0.24}Pd_{0.4}$/MIL-101 catalyst shows a good durability for dehydrogenation of $N_2H_4BH_3$ and N_2H_4. The excellent catalytic performance and durability may strongly encourage the practical application of $N_2H_4BH_3$ and $N_2H_4 \cdot H_2O$ as promising hydrogen storage materials.

Acknowledgments

This work was financially supported by the National Natural Science Foundation of China (Nos. 21463012 and 21763012) and the Natural Science Foundation of Jiangxi Province of China (Nos. 20171ACB21021 and 2016BAB203087).

Appendix A. Supplementary data

Supplementary data related to this article can be found at https://doi.org/10.1016/j.jallcom.2017.10.241.

References

[1] L. Schlapbach, A. Züttel, Hydrogen-storage materials for mobile applications, Nature 414 (2011) 353–358.
[2] Q.L. Yao, Z.H. Lu, W. Huang, X. Chen, Highly Pt-like activity of Ni-Mo/graphene catalyst for hydrogen evolution from hydrolysis of ammonia borane, J. Mater. Chem. A 4 (2016) 8579–8583.
[3] T. Umegaki, A. Seki, Q. Xu, Y. Kojima, Influence of preparation conditions of hollow silica-nickel composite spheres on their catalytic activity for hydrolytic dehydrogenation of ammonia borane, J. Alloys Compd. 588 (2014) 615–621.
[4] Q.L. Zhu, Q. Xu, Liquid organic and inorganic chemical hydrides for high-capacity hydrogen storage, Energy Environ. Sci. 8 (2015) 478–512.
[5] Z.H. Lu, J. Li, A. Zhu, Q.L. Yao, H. Huang, R. Zhou, R.F. Zhou, X. Chen, Catalytic hydrolysis of ammonia borane via magnetically recyclable copper iron nanoparticles for chemical hydrogen storage, Int. J. Hydrogen Energy 38 (2013) 5330–5337.
[6] Z.H. Lu, Q. Xu, Recent progress in boron- and nitrogen-based chemical hydrogen storage, Funct. Mater. Lett. 5 (2012) 1230001.
[7] C.W. Hamilton, R.T. Baker, A. Staubitz, I. Manners, B-N compounds for chemical hydrogen storage, Chem. Soc. Rev. 38 (2009) 279–293.
[8] R. Moury, G. Moussa, U.B. Demirci, J. Hannauer, S. Bernard, E. Petit, A.V.D. Lee, P. Miele, Hydrazine borane: synthesis, characterization, and application prospects in chemical hydrogen storage, Phys. Chem. Chem. Phys. 14 (2012) 1768–1777.
[9] Z.H. Lu, Q.L. Yao, Z.J. Zhang, Y.W. Yang, X. Chen, Nanocatalysts for hydrogen generation from ammonia borane and hydrazine borane, J. Nanomater. (2014) 729029.
[10] S. Karahan, M. Zahmakıran, S. Özkar, Catalytic methanolysis of hydrazine borane: a new and efficient hydrogen generation system under mild conditions, Dalton Trans. 41 (2012) 4912–4918.
[11] T. Hügle, M.F. Kühnel, D. Lentz, Hydrazine borane: a promising hydrogen storage material,, J. Am. Chem. Soc. 131 (2009) 7444–7446.
[12] Ç. Çakanyıldırım, E. Petit, U.B. Demirci, R. Moury, J.F. Petit, Q. Xu, P. Miele, Gaining insight into the catalytic dehydrogenation of hydrazine borane in water, Int. J. Hydrogen Energy 37 (2012) 15983–15991.
[13] S.L. Zhang, Q.L. Yao, Z.H. Lu, Synthesis and dehydrogenation of hydrazine borane, Prog. Chem. 29 (2017) 426–434.
[14] J. Hannauer, O. Akdim, U.B. Demirci, C. Geantet, J.M. Herrmann, P. Miele, Q. Xu, High-extent dehydrogenation of hydrazine borane $N_2H_4BH_3$ by hydrolysis of BH_3 and decomposition of N_2H_4, Energy Environ. Sci. 4 (2011) 3355–3358.
[15] J. Hannauer, U.B. Demirci, C. Geantet, J.M. Herrmann, P. Miele, Transition metal-catalyzed dehydrogenation of hydrazine borane $N_2H_4BH_3$ via the hydrolysis of BH_3 and the decomposition of N_2H_4, Int. J. Hydrogen Energy 37 (2012) 10758–10767.
[16] S. Karahan, M. Zahmakıran, S. Özkar, Catalytic hydrolysis of hydrazine borane for chemical hydrogen storage: highly efficient and fast hydrogen generation system at room temperature, Int. J. Hydrogen Energy 36 (2011) 4958–4966.
[17] Ç. Çakanyıldırım, U.B. Demirci, T. Şener, Q. Xu, P. Miele, Nickel-based bimetallic nanocatalysts in high-extent dehydrogenation of hydrazine borane, Int. J. Hydrogen Energy 37 (2012) 9722–9729.
[18] D.C. Zhong, K. Aranishi, A.K. Singh, U.B. Demirci, Q. Xu, The synergistic effect of Rh-Ni catalysts on the highly-efficient dehydrogenation of aqueous hydrazine borane for chemical hydrogen storage, Chem. Commun. 48 (2012) 11945–11947.
[19] D. Çelik, S. Karahan, M. Zahmakıran, S. Özkar, Hydrogen generation from the hydrolysis of hydrazine-borane catalyzed by rhodium(0) nanoparticles supported on hydroxyapatite, Int. J. Hydrogen Energy 37 (2012) 5143–5151.
[20] C.M. Li, Y.B. Dou, J. Liu, Y.D. Chen, S. He, M. Wei, D.G. Evans, X. Duan, Synthesis of supported Ni@(RhNi-alloy) nanocomposites as an efficient catalyst towards hydrogen generation from $N_2H_4BH_3$, Chem. Commun. 49 (2013) 9992–9994.
[21] S. Şencanlı, S. Karahan, S. Özkar, Poly(4-styrenesulfonic acid-co-maleic acid) stabilized nickel(0) nanoparticles: highly active and cost effective catalyst in hydrogen generation from the hydrolysis of hydrazine borane, Int. J. Hydrogen Energy 38 (2013) 14693–14703.
[22] Q.L. Yao, Z.H. Lu, Z.Z. Zhang, X.S. Chen, Y.Q. Lan, One-pot synthesis of core-shell Cu@SiO_2 nanospheres and their catalysis for hydrolytic dehydrogenation of ammonia borane and hydrazine borane, Sci. Rep. 4 (2014) 7497.
[23] D. Clémençon, J.F. Petit, U.B. Demirci, Q. Xu, P. Miele, Nickel- and platinum-containing core@shell catalysts for hydrogen generation of aqueous hydrazine borane, J. Power Sources 260 (2014) 77–81.
[24] N. Tunç, B. Abay, M. Rakap, Hydrogen generation from hydrolytic dehydrogenation of hydrazine borane by poly(N-vinyl-2-pyrrolidone)-stabilized palladium nanoparticles, J. Power Sources 299 (2015) 403–407.
[25] Q.L. Zhu, D.C. Zhong, U.B. Demirci, Q. Xu, Controlled Synthesis of ultrafine surfactant-free NiPt nanocatalysts toward efficient and complete hydrogen generation from hydrazine borane at room temperature, ACS Catal. 4 (2014) 4261–4268.
[26] Z.Z. Zhang, Z.H. Lu, X.S. Chen, Ultrafine Ni–Pt alloy nanoparticles grown on graphene as highly efficient catalyst for complete hydrogen generation from hydrazine borane, ACS Sustain. Chem. Eng. 3 (2015) 1255–1261.
[27] Z.Z. Zhang, Y.Q. Wang, X.S. Chen, Z.H. Lu, Facile synthesis of NiPt–CeO_2 nanocomposite as an efficient catalyst for hydrogen generation from hydrazine borane, J. Power Sources 291 (2015) 14–19.
[28] W. Ben Aziza, J.F. Petit, U.B. Demirci, Q. Xu, P. Miele, Bimetallic nickel-based nanocatalysts for hydrogen generation from aqueous hydrazine borane: investigation of iron, cobalt and palladium as the second metal, Int. J. Hydrogen Energy 39 (2014) 16919–16926.
[29] S. Karahan, S. Özkar, Poly(4-styrenesulfonic acid-co-maleic acid) stabilized cobalt(0) nanoparticles: a cost-effective and magnetically recoverable catalyst in hydrogen generation from the hydrolysis of hydrazine borane, Int. J. Hydrogen Energy 40 (2015) 2255–2265.
[30] Z.Z. Zhang, Z.H. Lu, H.L. Tan, X.S. Chen, Q.L. Yao, CeOx-modified RhNi nanoparticles grown on rGO as highly efficient catalysts for complete hydrogen generation from hydrazine borane and hydrazine, J. Mater. Chem. A 3 (2015) 23520–23529.
[31] Q.L. Yao, Z.H. Lu, K.K. Yang, X.S. Chen, M.H. Zhu, Ruthenium nanoparticles confined in SBA-15 as highly efficient catalyst for hydrolytic dehydrogenation of ammonia borane and hydrazine borane, Sci. Rep. 5 (2015) 15186.
[32] K.K. Yang, Q.L. Yao, W. Huang, X.S. Chen, Z.H. Lu, Enhanced catalytic activity of NiM (M = Cr, Mo, W) nanoparticles for hydrogen evolution from ammonia borane and hydrazine borane, Int. J. Hydrogen Energy 42 (2017) 6840–6850.
[33] J.M. Chen, Z.H. Lu, W. Huang, Z.B. Kang, X.S. Chen, Galvanic replacement synthesis of NiPt/graphene as highly efficient catalysts for hydrogen release from hydrazine and hydrazine borane, J. Alloys Compd. 695 (2017) 3036–3043.
[34] X.J. Gu, Z.H. Lu, H.L. Jiang, T. Akita, Q. Xu, Synergistic catalysis of metal-organic framework-immobilized Au-Pd nanoparticles in dehydrogenation of formic acid for chemical hydrogen storage, J. Am. Chem. Soc. 133 (2011) 11822–11825.
[35] J.P. Zhang, X.C. Huang, X.M. Chen, Supramolecular isomerism in coordination polymers, Chem. Soc. Rev. 38 (2009) 2385–2396.
[36] M. Yadav, Q. Xu, Catalytic chromium reduction using formic acid and metal nanoparticles immobilized in a metal-organic framework, Chem. Commun. 49 (2013) 3327–3329.
[37] M.C. Wen, Y.W. Cui, Y. Kuwahara, K. Mori, H. Yamashita, Non-noble-metal nanoparticle supported on metal-organic framework as an efficient and durable catalyst for promoting H_2 production from ammonia borane under visible light irradiation, ACS Appl. Mater. Interfaces 8 (2016) 21278–21284.
[38] M. Eddaoudi, J. Kim, N. Rosi, D. Vodak, J. Wachter, M. O'Keeffe, O.M. Yaghi, Systematic design of pore size and functionality in Isoreticular MOFs and their application in methane storage, Science 295 (2002) 469–472.
[39] H.L. Jiang, T. Akita, T. Ishida, M. Haruta, Q. Xu, Synergistic catalysis of Au@Ag core-shell nanoparticles stabilized on metal-organic framework, J. Am. Chem. Soc. 133 (2011) 1304–1306.
[40] H.L. Liu, L.N. Chang, C.H. Bai, L.Y. Chen, R. Luque, Y.W. Li, Controllable encapsulation of "clean" metal clusters within MOFs through kinetic modulation: towards advanced heterogeneous nanocatalysts, Angew. Chem. Int. Ed. 55 (2016) 5019–5023.
[41] A. Dhakshinamoorthy, H. Garcia, Catalysis by metal nanoparticles embedded on metal-organic frameworks, Chem. Soc. Rev. 41 (2012) 5262–5284.
[42] H.R. Moon, D.W. Lim, M.P. Suh, Fabrication of metal nanoparticles in metal-organic frameworks, Chem. Soc. Rev. 42 (2013) 1807–1824.
[43] J. Wang, Y. Li, Y. Zhang, Precious-metal-free nanocatalysts for highly efficient hydrogen production from hydrous hydrazine, Adv. Funct. Mater. 24 (2014) 7073–7077.

[44] J. Wang, X.B. Zhang, Z.L. Wang, L.M. Wang, Y. Zhang, Rhodium–nickel nanoparticles grown on graphene as highly efficient catalyst for complete decomposition of hydrous hydrazine at room temperature for chemical hydrogen storage, Energy Environ. Sci. 5 (2012) 6885–6888.
[45] S.K. Singh, A.K. Singh, K. Aranishi, Q. Xu, Noble-metal-free bimetallic nanoparticle-catalyzed selective hydrogen generation from hydrous hydrazine for chemical hydrogen storage, J. Am. Chem. Soc. 133 (2011) 19638–19641.
[46] T. Liu, J.H. Yu, H.Y. Bie, Z.R. Hao, Highly efficient hydrogen generation from hydrous hydrazine using a reduced graphene oxide-supported NiPtP nanoparticle catalyst, J. Alloys Compd. 690 (2017) 783–790.
[47] S.K. Singh, X.B. Zhang, Q. Xu, Room-temperature hydrogen generation from hydrous hydrazine for chemical hydrogen storage, J. Am. Chem. Soc. 131 (2009) 9894–9895.
[48] D.G. Tong, W. Chu, P. Wu, G.F. Gu, L. Zhang, Mesoporous multiwalled carbon nanotubes as supports for monodispersed iron–boron catalysts: improved hydrogen generation from hydrous hydrazine decomposition, J. Mater. Chem. A 1 (2013) 358–366.
[49] L. He, Y.Q. Huang, A.Q. Wang, X.D. Wang, X.W. Chen, J.J. Delgado, T. Zhang, A noble-metal-free catalyst derived from Ni-Al hydrotalcite for hydrogen generation from $N_2H_4 \cdot H_2O$ decomposition, Angew. Chem. Int. Ed. 51 (2012) 6191–6194.
[50] D.D. Wu, M. Wen, X.J. Lin, Q.S. Wu, C. Gu, H.X. Chen, A NiCo/NiO–CoO_x ultrathin layered catalyst with strong basic sites for high-performance H_2 generation from hydrous hydrazine, J. Mater. Chem. A 4 (2016) 6595–6602.
[51] D.G. Tong, D.M. Tang, W. Chu, G.F. Gu, P. Wu, Monodisperse Ni_3Fe single-crystalline nanospheres as a highly efficient catalyst for the complete conversion of hydrous hydrazine to hydrogen at room temperature, J. Mater. Chem. A 1 (2013) 6425–6432.
[52] F. Yang, Y.Z. Li, W. Chu, C. Li, D.G. Tong, Mesoporous Co–B–N–H nanowires: superior catalysts for decomposition of hydrous hydrazine to generate hydrogen, Catal. Sci. Technol. 4 (2014) 3168–3179.
[53] D.G. Tong, D.M. Tang, W. Chu, G.F. Gua, P. Wu, Synthesis of octahedral, truncated octahedral, and cubic Rh_2Ni nanocrystals and their structure–activity relationship for the decomposition of hydrazine in aqueous solution to hydrogen, Nanoscale 8 (2016) 7043–7055.
[54] M.C. Liu, Y.Q. Zheng, S.F. Xie, N.X. Li, N. Liu, J.G. Wang, M.J. Kim, L.J. Guo, Y.N. Xia, Facile synthesis of Pd-Ir bimetallic octapods and nanocages through galvanic replacement and co-reduction, and their use for hydrazine decomposition, Phys. Chem. Chem. Phys. 15 (2013) 11822–11829.
[55] S.K. Singh, Q. Xu, Complete conversion of hydrous hydrazine to hydrogen at room temperature for chemical hydrogen storage, J. Am. Chem. Soc. 131 (2009), 182032–218033.
[56] L. He, Y.Q. Huang, X.Y. Liu, L. Li, X.D. Wang, C.Y. Mou, T. Zhang, Structural and catalytic properties of supported Ni–Ir alloy catalysts for H2 generation via hydrous hydrazine decomposition, Appl. Catal. B Environ. 147 (2014) 779–788.
[57] K.V. Manukyan, A. Cross, S. Rouvimov, J. Miller, A.S. Mukasyan, E.E. Wolf, Low temperature decomposition of hydrous hydrazine over FeNi/Cu nanoparticles, Appl. Catal. A General 476 (2014) 47–53.
[58] D. Bhattacharjee, K. Mandal, S. Dasgupta, High performance nickel–palladium nanocatalyst for hydrogen generation from alkaline hydrous hydrazine at room temperature, J. Power Sources 287 (2015) 96–99.
[59] D. Bhattacharjee, S. Dasgupta, Trimetallic NiFePd nanoalloy catalysed hydrogen generation from alkaline hydrous hydrazine and sodium borohydride at room temperature, J. Mater. Chem. A 3 (2015) 24371–24378.
[60] H.L. Wang, J.M. Yan, S.J. Li, X.W. Zhang, Q. Jiang, Noble-metal-free NiFeMo nanocatalyst for hydrogen generation from the decomposition of hydrous hydrazine, J. Mater. Chem. A 3 (2015) 121–124.
[61] N. Cao, J. Su, W. Luo, G.Z. Cheng, Ni–Pt nanoparticles supported on MIL-101 as highly efficient catalysts for hydrogen generation from aqueous alkaline solution of hydrazine for chemical hydrogen storage, Int. J. Hydrogen Energy 39 (2014) 9726–9734.
[62] A.K. Singh, Q. Xu, Metal-organic framework supported bimetallic Ni-Pt nanoparticles as high-performance catalysts for hydrogen generation from hydrazine in aqueous solution, ChemCatChem 5 (2013) 3000–3004.
[63] J. Wang, W. Li, Y.R. Wen, L. Gu, Y. Zhang, Rh-Ni-B nanoparticles as highly efficient catalysts for hydrogen generation from hydrous hydrazine, Adv. Energy Mater. 5 (2015) 1401879.
[64] J.B. Yoo, H.S. Kim, S.H. Kang, B. Lee, N.H. Hur, Hollow nickel-coated silica microspheres containing rhodium nanoparticles for highly selective production of hydrogen from hydrous hydrazine, J. Mater. Chem. A 2 (2014) 18929–18937.
[65] J.M. Chen, Q.L. Yao, J. Zhu, X. Chen, Z.H. Lu, Rh-Ni nanoparticles immobilized on $Ce(OH)CO_3$ nanorods as highly efficient catalysts for hydrogen generation from alkaline solution of hydrazine, Int. J. Hydrogen Energy 41 (2016) 3946–3954.
[66] Z.J. Zhang, S.L. Zhang, Q.L. Yao, X. Chen, Z.H. Lu, Controlled synthesis of MOF-encapsulated NiPt nanoparticles toward efficient and complete hydrogen evolution from hydrazine borane and hydrazine, Inorg. Chem. 56 (2017) 11938–11945.